Atmospheric Environment 285 (2022) 119241

Contents lists available at ScienceDirect

Atmospheric Environment

journal homepage: www.elsevier.com/locate/atmosenv

A local marine source of atmospheric particles in the High Arctic

J.K. Nøjgaard [a,b,1,*], L. Peker [a,c,1], J.B. Pernov [a,d], M.S. Johnson [c], R. Bossi [a], A. Massling [a], R. Lange [a,e], I.E. Nielsen [a,f], A.S.H. Prevot [g], A.C. Eriksson [h,i], F. Canonaco [j], H. Skov [a]

[a] Department of Environmental Science, iClimate, Aarhus University, DK-4000, Roskilde, Denmark
[b] National Research Centre for the Working Environment, DK-2100, Copenhagen, Denmark
[c] Department of Chemistry, University of Copenhagen, 2100, Copenhagen, Denmark
[d] Extreme Environments Research Laboratory, École Polytechnique fédérale de Lausanne, 1951, Sion, Switzerland
[e] C.K. Environment A/S, DK-3500, Værløse, Denmark
[f] Danish Environmental Protection Agency, DK-5000, Odense, Denmark
[g] Laboratory of Atmospheric Chemistry, Paul Scherrer Institute (PSI), CH-5232, Villigen-PSI, Switzerland
[h] Division of Ergonomics and Aerosol Technology, Lund University, Box 118, SE-22100, Lund, Sweden
[i] Division of Nuclear Physics, Lund University, Lund, Box 118, SE-22100, Lund, Sweden
[j] Datalystica Ltd., Park innovAARE, 5234, Villigen, Switzerland

HIGHLIGHTS

- Factor analysis revealed 3 sources to Arctic aerosols: HOA, OOA and MOA.
- Marine Organic Aerosols (MOA) accounted for 18% in Spring/Summer Arctic aerosols.
- MOA correlated with Aitken mode particle mass.
- The local geographical origin of MOA was confirmed by back trajectories and source-receptor analysis.

ARTICLE INFO

Keywords:
ACSM
Aerosol
Aerosol mass spectrometry
Arctic
PMF

ABSTRACT

The chemical composition of non-refractory submicron aerosol (NR-PM_1) was characterized at the Villum Research Station (Villum) at Station Nord in North Greenland during spring-summer 2016 using a Time of Flight Aerosol Chemical Speciation Monitor (ToF-ACSM). The composition is dominated by sulfate (48%) and organic species (40%). Positive Matrix Factorization (PMF) identified three key factors corresponding to a primary hydrocarbon-like organic aerosol (HOA), and two types of secondary organic aerosol: oxygenated organic aerosol (OOA) and a marine organic aerosol (MOA). The HOA factor accounts for 5% of the organic aerosol mass, which is consistent with previous findings at Villum. The OOA factor accounts for 77% of the organic aerosol mass and correlates with accumulation mode particles, which supports previous findings indicating that oxidized organic aerosols are predominantly from long-range transport during winter and spring at Villum. The MOA factor was characterized by mass spectral fragments of methane sulfonic acid (MSA) from atmospheric oxidation of dimethyl sulfide, for which reason the MOA factor is considered to be of biogenic origin. MOA accounts for 18% of the organic aerosol mass and correlates with locally produced Aitken mode particles. This indicates that biogenic processes are not only a significant source of aerosols at Villum, but MOA also appears to be formed in the vicinity of the measurement site. This local geographical origin was confirmed through air mass back trajectory modelling and source-receptor analysis. During May, air masses frequently arrived from the east, with source regions for the MOA factor and therewith MSA located in the Barents Sea and Lincoln Sea with lesser contributions from the Greenland Sea. During June, air mass origin shifted to the west, with source regions for the MOA factor and MSA shifting correspondingly to Baffin Bay and the Canadian Arctic Archipelago. While shifting transport patterns between May and June lead to shifting source regions, sea ice likely played a role as well. During May, marginal ice zones were present in the Barents Sea between Svalbard and Franz Josef Land, while during June, sea ice in the northern part of Baffin Bay retreated and sea ice in the Canadian Arctic

* Corresponding author. National Research Centre for the Working Environment, DK-2100 Copenhagen, Denmark.
E-mail address: jkn@nfa.dk (J.K. Nøjgaard).
[1] Jakob Klenø Nøjgard and Lutfi Peker shares first authorship.

https://doi.org/10.1016/j.atmosenv.2022.119241
Received 24 February 2022; Received in revised form 27 May 2022; Accepted 14 June 2022
Available online 18 June 2022

Archipelago decreased. Although May and June experienced different transport patterns and sea ice conditions, levels of the MOA factor and MSA were similar between the months. This is likely due to similarities between marine biological activities in the Barents Sea and Baffin Bay. This research highlights the complex relationship between transport patterns, sea ice conditions, and atmospheric particle concentrations. Multiyear aerosol chemical composition from several High Arctic sites is encouraged to determine the full effects of ocean-atmosphere interactions and transport patterns on atmospheric aerosol concentrations.

1. Introduction

The Arctic is particularly sensitive to anthropogenic climate change, which has driven local temperature increase to three times the global mean during the last 100 years (Lenssen et al., 2019). Consequently, permafrost has been destabilized and the melting season extended leading to a critical decrease in sea-ice extent (Stroeve et al., 2007). These changes impact Earth's albedo and result in positive sea-ice and snow-albedo feedbacks, which further warms the Arctic (Lenton, 2012; Lenton et al., 2019). In addition to greenhouse gasses, atmospheric aerosols impact the radiation balance either directly by absorbing and scattering solar radiation or indirectly through aerosol-cloud interactions (Fan et al., 2016). Aerosols can impact the properties of clouds by serving as cloud condensation and ice nuclei (Twomey, 1977). A comprehensive characterization of the chemical composition and sources of aerosols is necessary to reduce uncertainties in Earth's energy budget and better understand their effects on climate change (IPCC, 2013, IPCC et al., 2021). Arctic aerosols show a distinct seasonal pattern with higher mass concentrations during late winter/early spring compared to summer and autumn. This phenomenon is referred to as Arctic Haze (Barrie et al., 1981; Heidam, 1984; Heintzenberg and Leck, 1994; Heidam et al., 1999, 2004; Quinn et al., 2007; Tunved et al., 2013; Nguyen et al., 2016). Higher concentrations of pollutants build up as the polar dome expands southwards (AMAP, 2011; Bozem et al., 2019) and provides greater accessibility to anthropogenic sources from outside the Arctic, particularly those emitted by industrial complexes in Eurasia. Furthermore, the strong temperature inversion and inefficient wet deposition slows removal processes resulting in a longer atmospheric lifetime for aerosols (Stohl, 2006; Sodemann et al., 2011; AMAP, 2011). Organic Aerosol (OA) typically comprises 1/3 or less of the sub-micron mass in the Arctic, but relatively few studies have provided detailed characterization of OA (Barrett et al., 2015; Brock et al., 2011; Frossard et al., 2011; Kawamura et al., 2010; Quinn et al., 2002; Shaw et al., 2010; Leaitch et al., 2018; Chang et al., 2011; Willis et al., 2018). Winter and spring are dominated by accumulation mode particles due to long-range transport. Relatively constant or even decreasing concentrations of OA are found during winter, while OA increases over the spring, suggesting that there is photochemical production of OA (Willis et al., 2018). Indeed, ultrafine particles are observed during summer and autumn, when local sources prevail (Nguyen et al., 2016). However, more detailed studies of the composition of OA in the Arctic is needed to understand the main sources and their variation (Willis et al., 2018).

In a recent study, we showed how the sub-micrometer ambient particle concentration, measured by a Soot Particle Aerosol Mass Spectrometer (SP-AMS), and its chemical composition changed from a mean of 2.3 μg m^{-3} in February at the onset of the Arctic Haze period, to 1.2 μg m^{-3} in May (Nielsen et al., 2019). In this period, biogenic sources became relatively more important than anthropogenic sources. In terms of chemical composition, sulfate (SO_4^{2-}) was the major component, comprising 66% of the non-refractory PM_1, followed by organics, accounting for 24% of PM_1. Using Positive Matrix Factorization (PMF) (Ulbrich et al., 2009; Zhang et al., 2011) and more specifically the PMF Evaluation Tool Software (PET, v2.08D; available online at http://cires1.colorado.edu/jimenez-group/wiki/index.php/PMF-AMS_Analysis_Guide), Nielsen et al. (2019) found that three factors explain the observed organic Aerosol (OA). First, Hydrocarbon-like Organic Aerosol (HOA, anthropogenic), characterized by hydrocarbon fragments from chemically reduced organic emissions and attributed to primary combustion sources of liquid, usually mostly fossil origin. The HOA was similar to another Arctic HOA factor found in Frossard et al. (2011), and was relatively more abundant at the onset of the campaign, where the long-range transport of aerosols was favoured. Second, Arctic Haze Organic Aerosols (AOA) and third, Marine Organic Aerosols (MOA, biogenic) were identified in the factor analysis. It was demonstrated that AOA dominated OA in the early spring (64–81% of OA), while the biogenic factor MOA dominated OA from April to May (24–74% of OA). At that time, ambient temperatures increased from −28.7 ± 5.8 °C (February mean ± standard deviation) to −14.7 ± 3.2 °C (May mean ± standard deviation), and the polar dome started to contract. Since transport into the dome is hindered, anthropogenic sources give low contributions in the late spring/summer months and total aerosol mass concentrations are consequently low. For climate models, the use of Arctic aerosol chemical composition is essential to improve future predictions of anticipated climate (Regayre et al., 2020). More knowledge is critically needed concerning the chemical composition and sources of summer aerosols, including answers to the most pressing questions regarding which sources are susceptible to climate change and especially identify the most important feedback mechanisms.

The Arctic is changing rapidly and thus it is of uppermost importance to understand and assess the composition of aerosols to predict future directions of aerosol compositions. In this paper, we present a two-month time series of ACSM measurements where we attempt to address contributing sources of Arctic aerosols by describing the levels and geographical origins of Arctic OA in spring and early summer and their relation to sea ice.

2. Materials and methods

2.1. Sampling site and period

The Short-lived Climate Forcers (SLCFs) campaign was conducted at the Villum Research Station (Villum) located at the Danish military facility Station Nord (Fig. S1) in North Greenland (81°36′N, 16°40′W, 24 m above mean sea level) and extended over 8 weeks from the beginning of May to the end of June 2016. Villum is in a region with a dry and cold climate where annual precipitation is 188 mm, and the annual mean temperature is −21 °C. The dominant wind direction is from the southwest with an average wind speed of 4 m s^{-1}. The measurement site is located 2 km southeast of the military facility, in the following named the "Air Observatory".

2.2. Instrumentation and analysis

Particle phase compounds for offline analysis were sampled using a custom build Filter Pack sampler, which was operated at 40 l/min and contained 7 filters, which were changed daily (Heidam et al., 2004; Skov et al., 2006; Nguyen et al., 2013). The exposed filters (40 mm nitrocellulose) were shipped to Aarhus University in Denmark and analyzed for a range of elements using Inductively Coupled Plasma – Mass Spectrometry (ICP-MS, Agilent 7900) and ions using a Metrohm Ion Chromatography (IC) system. A high-volume sampler (HVS) from Digitel (DHA-80) provided quartz filter samples for additional off-line analysis, including Thermal-optical analysis (Sunset laboratory, Lab OC-EC Aerosol analyzer) of Elemental Carbon (EC) and Organic Carbon

(OC). It is customary to sample OC on two filters in tandem in order to correct for sample artefacts related to absorption of semi volatile organic compounds (Cavalli et al., 2010), but only one filter is applied in the sample setup. For this reason, particulate OC may be slightly overestimated, but most likely to a lesser extent as indicated by the prevailing low VOC concentrations (Pernov et al., 2021). Particle number size distributions were measured using a TROPOS-type Scanning Mobility Particle Sizer as described in Wiedensohler et al. (2012). The setup enables analysis of aerosol particle diameters from 9 to 915 nm and the time resolution of the instrument is 5 min, including up- and down-scan. The SMPS was specifically designed for long-term operation with minimum maintenance as described in Nguyen et al. (2016).

A ToF-ACSM (Aerodyne Research) was deployed at Villum to measure non-refractory submicron aerosol species (organics, nitrate (NO_3^-), SO_4^{2-}, ammonium (NH_4^+) and chlorine (Cl) at a time resolution of 10 min, which was averaged to 1 h resolution (Fröhlich et al., 2013). The instrument was attached to a special heated particle inlet designed by TROPOS, Leipzig, Germany to minimize losses in the sample line. Briefly, the ToF-ACSM applies an aerodynamic lens to sample and focus submicron particles in a narrow beam into a differentially pumped vacuum chamber where gas molecules tend to diverge from the beam path. Under ambient conditions, the transmission of the aerodynamic lens is 100% for aerodynamic particle diameters between 150 nm and 450 nm, but less than 15% for particle diameters >1 μm (Liu et al., 2007). At the end of the vacuum chamber, the aerosol beam impacts a tungsten surface at 600 °C where non-refractory particulate matter is flash vaporized. The evolved species are ionized using a 70 eV electron impact (EI) ionizer. The ions are introduced into a Time-of-Flight mass analyzer using pulsed extraction and detected with a dynode detector from SGE. The mass spectra can be assigned to the organic fraction and several inorganic components based on knowledge of typical mass spectral fragmentation patterns (Allan et al., 2004). The mass concentration of organic and inorganic species is calculated based on signals, which are converted to organic matter, NO_3^-, SO_4^{2-}, NH_4^+ and Cl concentrations. Ionization efficiencies (IE) for NO_3^- and NH_4^+ were determined based on on-site calibrations using ammonium nitrate. Relative ionization efficiencies for Cl (1.3), SO_4^{2-} (1.2) and organics (1.4) were adopted from Canagaratna et al. (2007). The mass concentrations were processed from raw ToF-ACSM data by the Tofware version 2.5.13 software using Igor Pro version 6.37, according to the procedure described in Ng et al. (2011). A correction factor known as the collection efficiency (CE) is widely used in AMS and ACSM studies (Canagaratna et al., 2007) to account for particle losses in the vaporizer. This parameter depends on the chemical composition and in particular the acidity and the water content of the aerosol (Matthew et al., 2008). In this work, a time-dependent CE averaging 0.85 was determined using the approach described by Middlebrook et al. (2012), which is similar to a previous study at the same location in 2015 using an SP-AMS (Nielsen et al., 2019). To reduce the effect of ambient water content on the collection CE, a Nafion drier (Aerodyne Research) was connected to the ACSM inlet. A dedicated Sample line flow controller (Aerodyne Research) was connected to the ACSM sample line prior to the aerodynamic inlet and was operated at a recommended flow of 3.0 l/min.

2.3. Source apportionment of OA

Sources of Arctic aerosols were apportioned by analysing the ACSM mass spectral data with Positive Matrix Factorization (PMF). PMF is a bilinear model used to describe aerosol mass spectral data as a linear combination of source (factor) profiles and their time series (Paatero and Tapper, 1994; Canonaco et al., 2013). PMF has been used in several AMS and ACSM studies (e.g. Guo et al., 2020; Avery et al., 2019; Rattanavaraha et al., 2017; Timonen et al., 2016; Schlag et al., 2016; Fröhlich et al., 2015; Ripoll et al., 2015; Budisulistiorini et al., 2013; Nielsen et al., 2019), and recently a study of VOCs in the High Arctic (Pernov et al., 2021). The bilinear factor model in matrix notation can be described in Eq. (1), below.

$$\mathbf{X} = \mathbf{GF} + \mathbf{E} \tag{1}$$

Where the measured matrix **X** (consisting of *i* rows of *m/z* spectra corresponding to a given time and *j* columns of *m/z* values) is approximated by the product of matrices **G** and **F.** In terms of ACSM mass spectral data, **X, G, F, and E** correspond to the measured mass spectrum, factor time series, factor profiles, and model residuals, respectively. The entries in **G** and **F** are fit using a least squares algorithm that iteratively minimizes the objective function *Q* (Canonaco et al., 2013). *Q* is defined as the sum of the square of the residuals (e_{ij}) weighted by their measurement uncertainty (σ_{ij}) (Canonaco et al., 2013) as shown in (Eq. (2)).

$$Q = \sum_{i=1}^{n}\sum_{j=1}^{m}\left(\frac{e_{ij}}{\sigma_{ij}}\right)^2 \tag{2}$$

In this study, PMF analysis was applied up to *m/z* 100 using the multilinear engine (ME-2) running under toolkit SoFi (Source Finder) version 6.39 described in Canonaco et al. (2013). One important feature of ME-2 is that the user can apply *a priori information* on the factors, e.g., by adjusting the so-called *a*-value or sensitivity parameter (Eq. (3)). The *a*-value determines the extent to which the output profiles can differ from the input profile:

$$f_{j,\ solution} = f_j \pm a \times f_j \tag{3}$$

where *f* represents the factor profile and *j* indicates *m/z*. Thereby, the user can constrain one or more factors using the *a*-value. In this study, we performed both unconstrained and constrained runs for solutions with the numbers of factors varying from 2 to 5. We observed that one of the factors, the HOA factor, was not completely separated from the other factors in unconstrained runs. Therefore, we constrained the HOA factor by using the HOA reference mass spectrum obtained at the same location in the CRAICC campaign one year earlier using an SP-AMS (Nielsen et al., 2019). Data points where $e_{ij} \gg \sigma_{ij}$ have a large impact on the number of PMF model iterations. To prevent the solution from being influenced by these effects, data points must be treated accordingly., The model was run in robust mode, which eliminates the impact of strong outliers, which were defined as having a residuals-to-measurement ratio (α) exceeding a default value of 4. In addition, *m/z* values with a signal-to-noise ratio (S/N) below 0.2 were down-weighted by a factor of 10, and those with S/N between 0.2 and 1 were down-weighted by a factor of 3, as described by Ulbrich et al. (2009).

2.4. Back trajectory and source-receptor analysis

To characterize the air mass history and locate source regions, the R package Openair (Carslaw and Ropkins, 2012) was utilized to produce trajectory frequency and potential source contribution function (PSCF) maps on a 2° latitude by 2° longitude grid. Trajectories in Openair were calculated using the HYSPLIT model (Draxler and Hess, 1998; Rolph et al., 2017) at 50 m arrival altitude and 120 h backwards in time using Global NOAA-NCEP/NCAR reanalysis data archives on a 2.5° resolution. Trajectory frequencies were calculated for each grid cell, which shows the frequency of back trajectory points in each grid square normalized by the total number of trajectories multiplied by 100%. A PSCF, shown in Eq. (4), calculates the probability that an emission source is in a grid cell of latitude *i* and longitude *j*, on the basis that emitted material in the gird cell *ij* can be transported along the trajectory and reach the receptor site (Ashbaugh et al., 1985).

$$PSCF = \frac{m_{ij}}{n_{ij}} \tag{4}$$

Where n_{ij} is the number of times a trajectory has passed through grid cell *ij* and m_{ij} is the number of times that a concentration was above a certain threshold value, in this case, the 75th percentile. To account for

uncertainty in cells with a small number of trajectories passing through, a weighting function was applied (Carslaw and Ropkins, 2012).

3. Results and discussion

3.1. Time series

The time-dependent concentrations of organic species, SO_4^{2-}, NO_3^-, NH_4^+ and Cl measured by the ToF-ACSM are presented in Fig. 1. The sum of these species makes up the non-refractory part of submicron particulate matter, in the following called NR-PM_1, which by definition flash vaporizes in the ACSM vacuum region at temperatures of 600 °C. Offline measurements were also conducted (section 3.2). NR-PM_1 averages 0.57 μg m^{-3} over the entire campaign period of which SO_4^{2-} accounts for 48% and organics 40%. Nielsen et al. (2019) reported average submicron aerosol mass concentrations of 2.3–3.3 μg m^{-3} in February–April, and 1.2 μg m^{-3} in May, which is similar to the average of 1.05 μg m^{-3} in the first week of May in this study (Table S1). In the present study, NR-PM_1 is close to the SMPS derived mass concentration of PM_1, based on integrated particle volume size distributions calculated from particle number size distributions during May and June 2016, and applying an average density of 1.6 to obtain particulate mass ($R^2 = 0.84$, $y = 1.01$ x). In general, the data shows that particle sizes between 40 and 400 nm account for virtually all submicron mass (Lange et al., 2018). Furthermore, the ToF-ACSM has close to 100% transmission efficiency for particles in the range of 150 nm–450 nm (Fröhlich et al., 2013) and the measured species are the most abundant ones in terms of mass. The masses not accounted for are particulate water, NaCl, and elements such as K, Ca, Si, Al and Fe and their inorganic counter ions (Heidam et al., 2004; Nguyen et al., 2013). In addition, refractory carbonaceous species are not measured by the ToF-ACSM. In this group of species, black carbon (BC) has been measured in concentrations of only a few tenths of ng m^{-3} in late spring during the Arctic haze period, though peaks up to 100 ng m^{-3} are encountered (Nielsen et al., 2019). Therefore, not more than 10% in mass originating from BC on average during Arctic haze periods is expected. As expected from the remote location of Villum, we did not observe a distinct diurnal pattern for the chemical species (Fig. 1), which suggests long-range transport to be the predominant source of aerosols at this time of year. This consistent with previous findings (Heidam et al., 2004; Nguyen et al., 2013; Nielsen et al., 2019).

During the campaign, SO_4^{2-} averaged 0.28 ± 0.22 μg m^{-3} equal to about 48% of NR-PM_1. Sulfate being a major aerosol component is consistent with previous findings at Villum based on lower time-resolution measurements, where e.g. Fenger et al. (2013) reported 0.54–1.09 μg m^{-3} in March 2009, and Nielsen et al. (2019) reported SO_4^{2-} to account for 66% of the submicron aerosol mass using a SP-AMS. Previous studies indicate that atmospheric SO_4^{2-} occurs from mainly

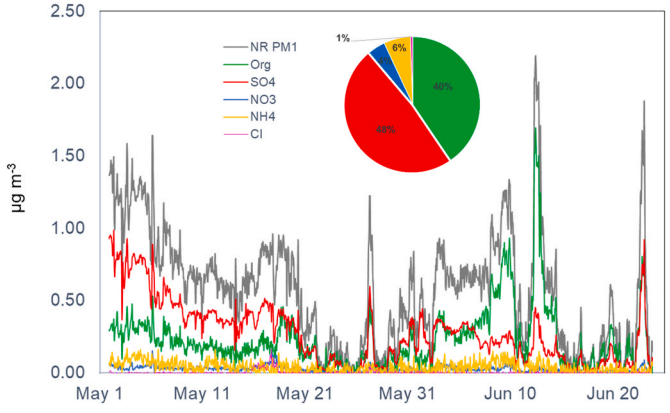

Fig. 1. Time series for organics, SO_4^{2-}, NO_3^-, NH_4^+ and Cl^- and the sum of non-refractory species NR- PM_1.

secondary processes, whereas the contribution from primary emissions is minor (Heidam et al., 2004). Additionally, SO_4^{2-} and its main precursor SO_2 is predominantly anthropogenic and arrives due to long-range transport from source regions in Siberia (Heidam et al., 2004; Hirdman et al., 2010; Nguyen et al., 2013). Emissions of dimethyl sulfide (DMS) from marine environments and following tropospheric oxidation is an important source of SO_4^{2-} from natural sources/processes, in particular during summer when the polar dome contracts and hinders the transport of anthropogenic pollution into the area (Pernov et al., 2021) (however, we have to remember that during summer the SO_4^{2-} concentration is much lower compared to winter and spring). Nielsen et al. (2019) reported a Marine Organic Aerosol factor (MOA), which emerged at Villum in late March and prevailed until the end of May. The MOA factor accounted for 22% of the organic aerosol as an average over the campaign. However, the contribution of biogenic emissions is minor during winter and early spring due to the sea-ice-covered ocean around the receptor site (Heidam et al., 2004; Pernov et al., 2021). Nielsen et al. reported a markedly decrease in SO_4^{2-} from April to May using an SP-AMS (2019). In the current study, which proceeds further into June, we observed a higher SO_4^{2-} concentration during May, averaging 0.35 ± 0.24 μg m^{-3} (Table S1) and only about half of this concentration was observed in June (0.19 ± 0.14 μg m^{-3}). A further contraction of the polar dome and the consequently impaired long-range transport of anthropogenic emissions combined with the onset of precipitation likely explains this drop in SO_4^{2-}. Biogenic emissions of DMS from the ocean were expected to impact the aerosol concentration since a lower sea ice extent during summer (Dall'Osto et al., 2018a; Pernov et al., 2021) implies a larger surface area for emissions from DMS-producing marine organisms to escape into the atmosphere (Carpenter et al. 2012; Nielsen et al., 2019, Dall'Osto et al., 2018b).

During our study, organic particulate matter makes the second largest contribution to NR-PM_1 with an overall average of 0.23 ± 0.21 μg m^{-3} corresponding to 40% of the total mass concentration during the beginning of May to the end of June 2016. While SO_4^{2-} decreased in June, organic species increased from 0.18 ± 0.11 μg m^{-3} in May (30%) to 0.30 ± 0.29 μg m^{-3} in June (55%). SO_4^{2-} is the major component, while organics are the minor component from May 2nd to May 17th, a period which is typically still dominated by Arctic haze. In the period from May 18th to June 6th SO_4^{2-} and organics are found in similar concentrations and organics dominate from June 7th to June 14th. While the first period is linked to the transition phase between Arctic haze and spring, regional emissions dominate the aerosol population in the High Arctic during summer.

The concentration of NO_3^- is very low compared to SO_4^{2-} and organics and averages only 4% of NR-PM_1 during the campaign (0.024 ± 0.021 μg m^{-3}) (Fig. 1). This is consistent with previous results reported at Villum (Nguyen et al., 2013). In late winter/early spring, NO_3^- in the fine mode (<1 μm) originates mainly from long-range transport, while coarse mode (>1.5 μm) NO_3^- was hypothesized to originate from more local/regional sources, with frost flowers being proposed as a possible source under high wind speeds (Fenger et al., 2013). Contributions from NH_4^+ and Cl to aerosol mass were typically at or below the detection limit (Table S4) with an average concentration of 0.037 ± 0.042 and 0.003 ± 0.015 μg m^{-3}, respectively.

3.2. Comparison with other measurements

A collection efficiency (CE) factor of 0.85 was applied to account for particle losses in the vaporizer, which is related to aerosol acidity (Canagaratna et al., 2007; Middlebrook et al., 2012). The acidic level was determined using the ratio of measured NH_4^+ to predicted NH_4^+ (NH_4^+ pred) which would be needed to neutralize the major inorganic anions measured by ToF-ACSM (Middlebrook et al., 2012). Previous studies in the Arctic showed time-dependent CE's ranging between 0.8 and 1 (Nielsen et al., 2019; Frossard et al., 2011). NR-PM_1 was compared to the mass concentration calculated from SMPS measurements of particle

mobility diameters (9–915 nm) in the Air Observatory. The SMPS volume concentration was calculated and converted to mass concentration using an estimated density of 1.6 μg m^{-3} based on the fractional contribution of sulfuric acids ($\rho_{sulfate}$ = 1.84 μg m^{-3}) and organics ($\rho_{org,\ aged}$ = 1.27 μg m^{-3}) (Fröhlich et al., 2013). The derived mass concentrations from both instruments were strongly correlated (R^2 = 0.84) with a slope of 1.01 (Fig. S2) for an identical period.

ToF-ACSM measurements of organics, SO_4^{2-}, NO_3^- and NH_4^+ were converted to weekly averages and compared to the weekly averages obtained from off-line Total Suspended Particle (TSP) filter measurements in the same period (see supplementary material, Table S1). ToF-ACSM averages of NO_3^- and NH_4^+ concentrations were both extremely low, 0.02 and 0.04 μg m^{-3}, respectively. The ToF-ACSM reports organic matter (OM) mass concentration, which is taking into account the mass concentration of hydrogen, oxygen and other atoms present in organic species. Conversely, thermal optical measurements (Birch, 1998; Cavalli et al., 2010) of Organic Carbon (OC) reports only the mass concentration of carbon. In order to compare off-line thermal optical measurements of OC to ToF-ACSM measurements of organics, an OM/OC conversion factor must be applied. An OM/OC conversion factor of 2.1 has been recommended by Turpin and Lim (2001). This was supported in a previous measurement campaign at Villum in Spring 2015, where the major sources to organic aerosols showed OM/OC ratios of 2.0 and 2.4 (Nielsen et al., 2019). By application of an OM/OC conversion of 2.1 in this campaign, a good agreement was found between the average concentration of organics measured by the ToF-ACSM and OM calculated from OC measured by thermal-optical analysis. However, ToF-ACSM measurements of SO_4^{2-} were less consistent with offline measurements in this campaign. In fact, the average SO_4^{2-} concentration was 40% lower than those obtained from the ToF-ACSM. On average for this campaign period, the sum of SO_4^{2-}, organics, and NH_4^+ obtained from filter measurements as TSP was 23% lower than the average NR- PM_1 measured by the ToF-ACSM.

3.3. Source apportionment of organic aerosol

The unit mass resolution (UMR) organic aerosol data was analyzed using SoFi version 6.93, which is based on the ME-2 engine. PMF runs were tested with 2–5 factors, and $Q/Q_{expected}$ decreased in going from 2 to 3 factors, from 3 to 4 factors and from 4 to 5 factors (Fig. S3). However, the change from 4 or 5 factors did not identify any new factors likely to reflect new sources. A three-factor solution returned the best result, in agreement with Nielsen et al. (2019): i.e., a Hydrocarbon-like Organic Aerosol (HOA), an Oxygenated Organic Aerosol (OOA) and a Marine Organic Aerosol (MOA). Each factor is characterized by a distinct time series and a mass spectral profile, which is characteristic of the source origin or mechanism of formation (Figs. 2 and 3).

The HOA factor was constrained using a HOA factor from Nielsen et al. (2019). a-values (in equation (3)) in the range from 0.05 to 0.20, where a = 0 corresponds to a fully constrained factor (Canonaco et al., 2013), were tested in accordance with Crippa et al. (2014). The HOA factor accounted for 4.6% of OA in the more constrained run with a = 0.05 (Table S2). However, comparable HOA values were obtained with a-values of 0.1, 0.15 and 0.2 which yielded a HOA factor contribution of 4.9–5.2%. Since the HOA factor was adopted from a previous campaign at Villum in 2015, where meteorological conditions and thereby source origin could be different from those in the present campaign, a less constrained *a*-value of 0.2 was selected. The HOA profile is characterized by a fragmentation pattern corresponding to aliphatic hydrocarbons, in particular at *m/z* 27, 41, 43, 55, 57, 67, 69, 71 ($C_3H_5^+$, $C_3H_7^+$, $C_4H_7^+$, $C_4H_9^+$, $C_5H_7^+$, $C_5H_9^+$ and $C_5H_{11}^+$, respectively) and aromatic compounds (Canagaratna et al., 2007; Aiken et al., 2009). Furthermore, *m/z* 44 (CO_2^+) is minor (Fig. 2), and there is a high peak at *m/z* 57 ($C_4H_9^+$), which characterizes primary combustion sources of fossil fuel (Zhang et al., 2005; Aiken et al., 2009; Frossard et al., 2011). The absence of markers of levoglucosan at *m/z* 60 ($C_2H_4O_2^+$) and *m/z* 73 ($C_3H_5O_2^+$) indicates an origin from fossil fuels which is not mixed with wood combustion. However, measured concentrations of biomass burning organic aerosols based on levoglucosan are often low in the Arctic, which may reflect the atmospheric decomposition of the marker (Zangrando et al., 2013). In addition, wildfires, which may contribute with substantial amounts of both OA and EC to the Arctic aerosol population, are typically more frequent later in the summer and early autumn, however, wet deposition during transport can affect particulate levels (Pernov et al., 2021). In this study, HOA accounts for only 5% of OA averaged over the campaign (0.01 μg m^{-3}). This somewhat less than the abundance of the HOA factor accounting for 12% in a similar Arctic study (Nielsen et al., 2019). There are periods of a few days, e.g. June 8 to 10 and June 11 to 13, where HOA was markedly higher compared to the campaign average (Fig. 3c). While the spikes are most likely related to activities at Station Nord, other broader peaks correlate with organics which could be long-range transported. However, due to their low abundance in general, no effort was put into further analysis and cleaning of the data.

The second factor OOA accounts for 77% of OA (0.17 μg m^{-3}) and is the most oxygenated OA characterized by prominent peaks at *m/z* 44 (mainly CO_2^+) (and associated *m/z* 28 (CO^+), which indicates that this factor is likely strongly linked to Secondary Organic Aerosol (SOA) formation (See Fig. 2). In numerous studies from the Northern hemisphere, two different OOA factors were often identified, characterized by different O/C ratios as an indication of their average oxidation state (Jimenez et al., 2009). According to Jimenez et al. (2009), Semi Volatile Oxygenated Organic Aerosols (SV-OOA) currently denoted less oxygenated OOA (LO-OOA) are associated with relatively high volatility and a lower O/C-ratio (empirical formula $C_8H_{11}O_3$). Conversely, Low

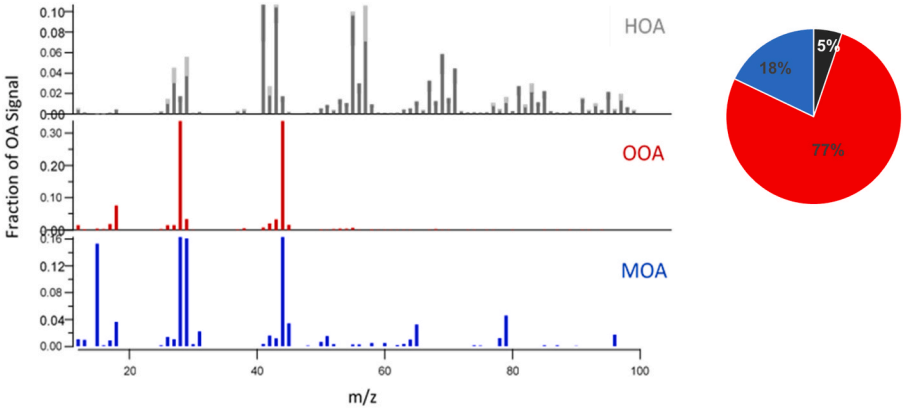

Fig. 2. PMF factor profiles of Hydrocarbon-like Organic Aerosols (HOA), Oxygenated Organic Aerosols (OOA) and Marine Organic Aerosols (MOA). The relative abundance of the factors is illustrated in the pie diagram.

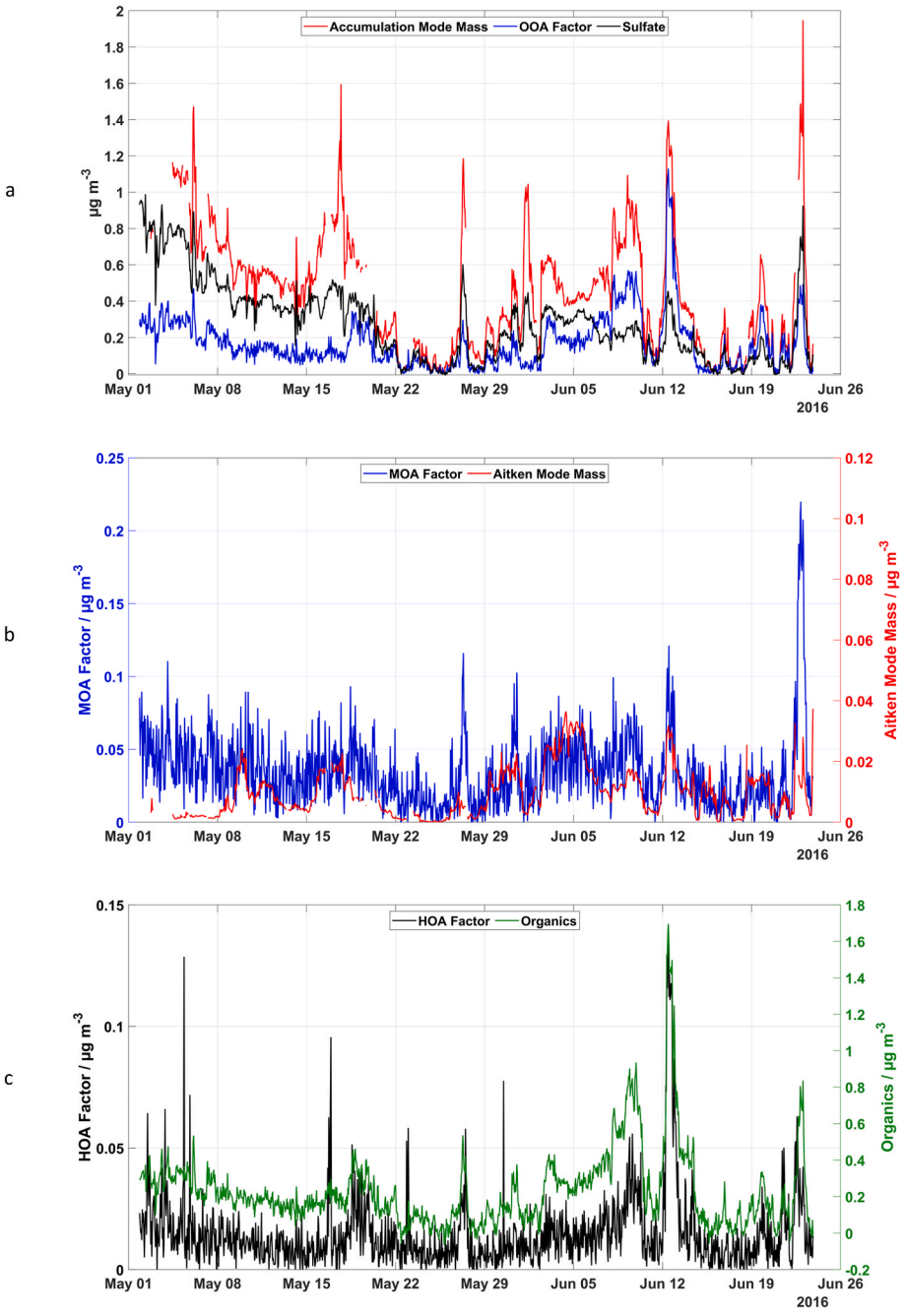

Fig. 3. Time series for a) the Oxygenated Organic Aerosol factor (OOA), accumulation mode mass concentration (80-900 nm) and SO_4^{2-}, b) Marine Organic Aerosol factor (MOA) and Aitken mode mass concentration (10-80 nm), and c) Hydrocarbon-like Organic Aerosol factor (HOA) and total organics (lower panel).

Volatility Oxygenated Organic Aerosols (LV-OOA) currently denoted more oxygenated OOA (MO-OOA) are associated with low volatility and higher O/C-ratio (empirical formula $C_8H_{10}O_{5.5}$). Although the ToF-ACSM does not provide information on the O/C-ratio, the less fragmented OOA (Fig. 2), also correlates well with SO_4^{2-} (Table S3), in particular from the end of May and onwards (Fig. 3). Hence, OOA can most likely be assigned to MO-OOA. This agrees with the continental factor identified by Chang et al. (2011) in the Central Arctic Ocean, and the Arctic Haze Organic Aerosol factor accounting for 66% of the aerosol mass identified in Nielsen et al. (2019) in Greenland, though OOA in this study is even less fragmented and is therefore presumably characterized by a higher average oxidation state. The implication is that 77% of the organic aerosol is not locally produced during May and June 2016 at Villum, but presumably transported over long-range distances. Earlier Arctic studies have identified mixed combustion sources to be responsible for more than 60% of the highly oxidized submicron organic aerosol mass (Frossard et al., 2011). Fig. 3a shows the time series of OOA and SO_4^{2-} during the campaign. OOA is the most abundant OA factor in both May (76%) and June (79%) and actually increases towards the end of June 2016. This is contrary to the situation in 2015, where the Marine Organic Aerosol became the dominant source of aerosols accounting for 75% of the aerosol mass in May (Nielsen et al., 2019), which reflects the large inter-annual variation of Arctic aerosol chemical composition observed at Villum and underlines the importance of studies of multi-year aerosol chemical composition. OOA is observed in a relatively high concentration (~0.3 µg m^{-3}) at the beginning of May and decreases to a minimum (~0.1 µg m^{-3}) at the end of May and increases again with several bursts (lasting several days) up to the end of June. Fig. 3a shows

the correlation between the OOA factor and accumulation mode mass concentration, in this study defined as particles with diameters exceeding 80 nm. OOA correlates well with accumulation mode mass concentration (Fig. 3a), indicating that this factor is probably the result of long-range transport to the station (Lange et al., 2018).

The Marine Organic Aerosol factor (MOA) accounts for 18% of OA (Figs. 2 and 3b), which is comparable to the abundance of 22% found by Nielsen et al. (2019) on the same location. However, a marine biogenic source accounting for 33% of the aerosol mass has previously been reported in a study on the central Arctic Ocean (Chang et al., 2011). As apparent from Fig. 2, the factor is dominated by *m/z* 44 (CO_2^+) (and the associated *m/z* 28 (CO^+) which is a fragment from the decomposition of carboxylic acids and their derivatives (Duplissy et al., 2011). Other characteristic peaks originate from MSA at *m/z* 15, 65, 78, 96 and the fragment ion $CH_3SO_2^+$ at *m/z* 79 (Huang et al., 2017). In a previous study at the same location (Nielsen et al., 2019) we identified a marine organic aerosol using a high-resolution AMS. A distinct peak characteristic for MOA was detected at m/z 78.9854 and corresponds to the fragment $CH_3SO_2^+$, which is characteristic for MSA (Huang et al., 2017). The fragment reveals that MOA has a secondary biogenic source (Becagli et al., 2013). MSA is mainly formed from oxidation of biogenically emitted dimethyl sulfide (DMS), i.e. from aqueous phase oxidation of DMS and subsequently partitions into the gas phase (Baccarini et al., 2021; Chen et al., 2018; Hoffmann et al., 2016). MOA remains relatively constant, though several minor bursts are observed during the campaign (Fig. 3b). Some correlation is observed between MOA and Aitken mode mass concentration, in this study defined as particles in the size range 30–80 nm. However, the correlation between the MSA fragment $CH_3SO_2^+$ and Aitken mode mass concentration was more clear (Fig. S4). Aitken mode particles have predominantly been observed in greater abundance during spring and summer at Villum and are known to originate from further growth of freshly nucleated particles (Lange et al., 2018; Nguyen et al., 2016). Direct emission of such particles would typically require local combustion sources, which are very scarce in the High Arctic, and particles from long-range transport typically process into the accumulation mode based on condensational ageing and cloud processing. Marine and cryospheric emissions favour the formation and growth of ultrafine aerosols (Sipilä et al., 2016; Beck et al., 2021; Dall'Osto et al., 2018a, b), although marine nanogels have been shown to be a primary source of Aitken mode particles from evaporating fog and clouds (Karl et al., 2013). The MOA factor is likely influenced by these sources, and the strong association of Aitken mode particles with the MOA factor shows that the MOA factor not only explains 18% of the organic aerosol, but also that local and regional sources to MOA are significant. Aitken mode particles can only be local of origin, since condensation and coagulation during long-range transport would cause Aitken mode particles to grow to larger sizes.

"Marine and coastal marine areas account for a large part of Arctic, where organic aerosols can be formed. For example, the production of primary marine aerosols is known to correlate with wind speed (Willis et al., 2018). in Arctic regions, primary organic particles are believed to consist of water-soluble or surface-active organic compounds, which are present in the surface water, or they could consist of water-insoluble microgels (Willis et al., 2018; Leck and Bigg, 2005; Orellana et al., 2011). Only the secondary marine source was identified in this study. However, further studies in the autumn season could perhaps clarify the role of primary marine organic aerosols in the Arctic, since the sea salt source has previously been found to peak during this season (Nguyen et al., 2013).

3.4. Source regions of the MOA factor and MSA and relationship with sea ice

To investigate the hypothesis that local and/or regional sources contribute significantly to the MOA factor, the geographical origin of the MOA factor and MSA $CH_3SO_2^+$ was examined through air-mass back trajectory modelling and source-receptor analysis. A trajectory frequency analysis was used to assess the general transport patterns and a PSCF was utilized to elucidate the source regions of the MOA factor and MSA. Only trajectory steps below the mixed layer were considered in these analyses, as marine biogenic emissions are most likely incorporated into air masses when extensive surface contact occurs. Over the entire campaign, air masses most frequently arrived from the Barents Sea, Greenland Sea, Baffin Bay, and the Canadian Arctic Archipelago (Fig. 4a). This pattern is generally consistent with the source regions of the MOA factor and MSA (Fig. 4d and g), although with decreased contributions from the Greenland Sea. When separating air mass trajectories by month, differences in origin are evident between May and June. Air masses arrived mainly from the east (the Barents and Greenland Sea) in May (Fig. 4b) and from the west (Baffin Bay and the Canadian Arctic Archipelago) in June (Fig. 4c). This shift in air origin between months is reflected in the source regions of the MOA factor and MSA (Figure e,f,h, i). The source regions of MOA in May are the Barents Sea and the Fram Strait, as well as contributions from the Lincoln Sea (Fig. 4e). For MSA in May, the source regions are the Barents Sea and the Lincoln Sea, with a lesser contribution from the Fram Strait compared to the MOA factor (Fig. 4h). In June when air mass origin shifts towards Baffin Bay and the Canadian Arctic Archipelago, the source regions for MOA shift correspondingly (Fig. 4f). For MSA in June, the predominant source region is Baffin Bay (Fig. 4i).

While differences in the general transport patterns in May and June resulted in different source regions for the MOA factor and MSA concentration between the two months, sea ice coverage could also play a role in the observed levels of the MOA factor and MSA concentration. Therefore, monthly merged sea ice concentrations were obtained for May and June 2016 from the National Snow and Ice Data Center (https://nsidc.org/data/G02202/versions/4) and compared to investigate differences in sea ice conditions. During May, the northeast coast of Greenland is ice-locked, although there is open water in the Greenland Sea southwest of Svalbard, and in the Barents Sea marginal sea ice zones are present between Svalbard and Franz Josef Land (Fig. 5a). Phytoplankton blooms, as early as April, have been observed in the marginal sea ice zone of the Barents Sea (Wassmann et al., 2006), which are likely induced by sea ice melt (Matrai et al., 2007). The resulting freshwater from the sea ice melt acts as an irradiated trap for micro-organisms and nutrients, isolating it from the more productive waters below (Galí and Simó, 2010). This is likely the mechanism responsible for the Barents Sea being a potential source region for the MOA factor and MSA in May. Marginal sea ice zones, which are favourable for algae blooms (Perrette et al., 2011) and DMS emission to the atmosphere (Leck and Persson, 1996), were present in the Barents Sea during May (Fig. 5a). During June, the marginal sea ice zones east of Svalbard largely disappear and sea ice around the Greenlandic coast decreases. Meanwhile in Baffin Bay, large areas of open water appear as well as a decrease in sea ice coverage in the Canadian Arctic Archipelago (Fig. 5b). Becagli et al. (2016) showed air masses exclusively arrive from Baffin Bay at Thule, Greenland, as well as significant correlations between MSA at Thule and Chlorophyll-a, primary production, and sea ice melt in Baffin Bay. This retreat in sea ice (and subsequent advance of the marginal ice zone), coupled with an increased amount of solar radiation and Chlorophyll-a in June likely contributed to the observed levels of the MOA factor and MSA at Villum during our study. Indeed, the largest DMS production in Baffin Bay occurs during May–June in the marginal sea ice zones (Becagli et al., 2016). During the NETCARE research cruises in the summer (July and August) of 2014 and 2016, higher concentrations of nanoparticles were observed in the northern parts of Baffin Bay in 2016. Differences in environmental factors between the campaigns revealed that a lower condensation sink, higher solar radiation, decreased sea ice coverage, and differences in local marine biological activity, collectively or individually contributed to the increased levels of nanoparticles between the years in 2014 and 2016 (Collins et al., 2017). They highlighted the importance of marine microbial processes on the behaviour

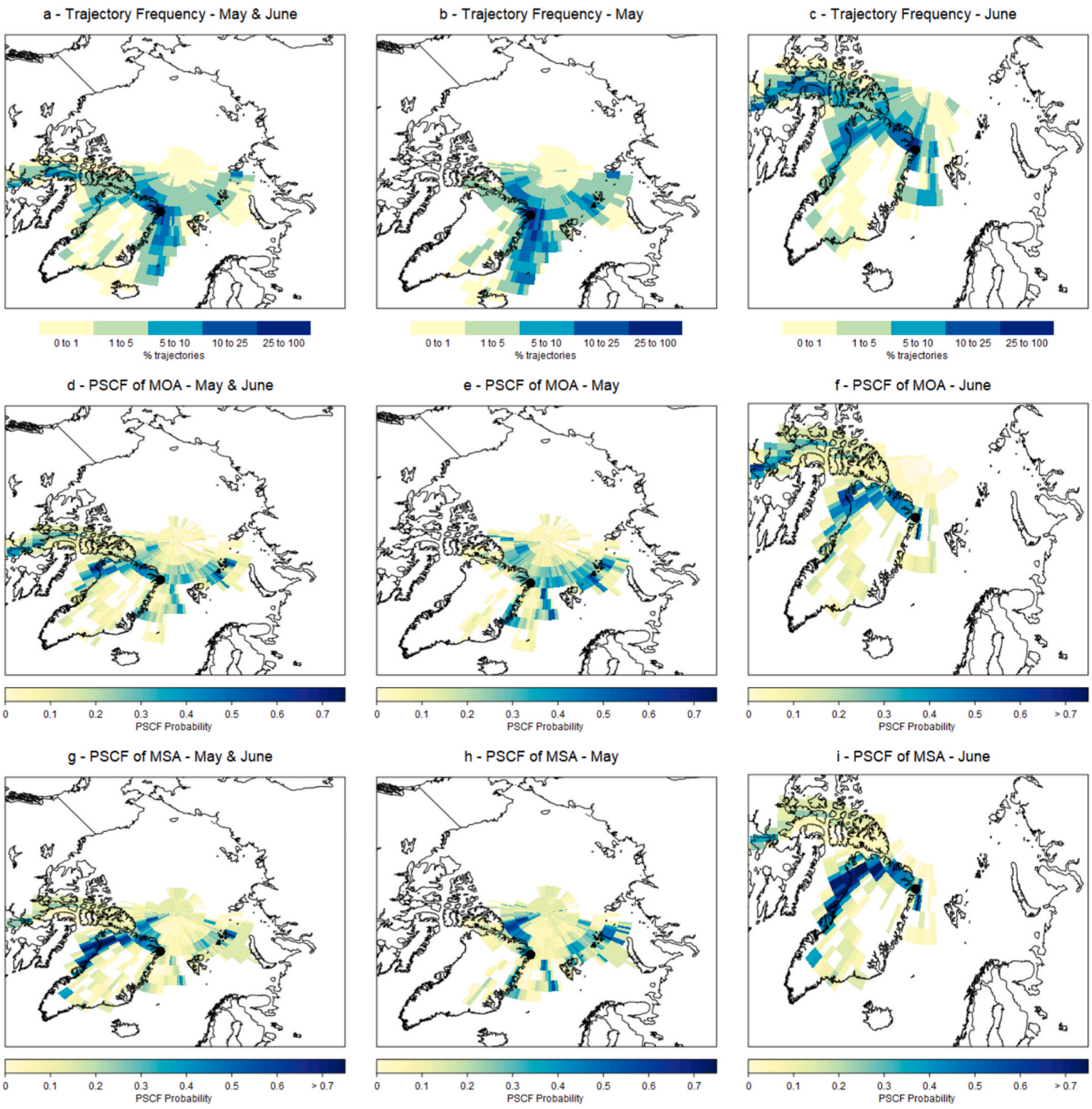

Fig. 4. Plots of a-c) back trajectory frequencies and Potential Source Contribution Function (PSCF) maps of d-f) MOA and g-i) MSA on a 2° latitude by 2° longitude grid.

and occurrence of ultrafine particle formation and growth.

Although air masses frequently arrived from the Greenland Sea and Barents Sea in May, the Greenland Sea was not a major source region for either the MOA factor or MSA. This is likely due to differences in biological activity in the two seas. Lee et al. (2020) showed that during May 2016–2018, the Barents Sea is a major source region for Chlorophyll-a, with lesser contributions from the Greenland Sea. Becagli et al. (2016) showed the peak of Chlorophyll-a in the Barents Sea occurs in late April or May, corresponding to the start of the sea ice melt, and that in the Greenland Sea primary production is related to pelagic blooms and not marginal sea ice zone blooms (Becagli et al., 2016). The maximum MSA concentrations at Ny-Ålesund occur in May (Becagli et al., 2019). Conversely, later in the summer, the Greenland Sea becomes the dominant source region of Chlorophyll-a (Becagli et al., 2016, 2019; Lee et al., 2020; Park et al., 2018), and becomes a source of DMS and carboxylic acids at Villum (Pernov et al., 2021). The taxonomic differences between phytoplanktonic assemblages in the Barents Sea and Greenland Sea are the likely cause of different source strengths between the two seas (Becagli et al., 2016).

Interestingly, concentrations of the MOA factor and MSA were similar between May and June (0.033 ± 0.021 and 0.036 ± 0.031 μg m^{-3}, respectively) even though transport patterns shifted from east to west and sea ice conditions in the source regions were different between months. This is probably due to similarities between phytoplanktonic

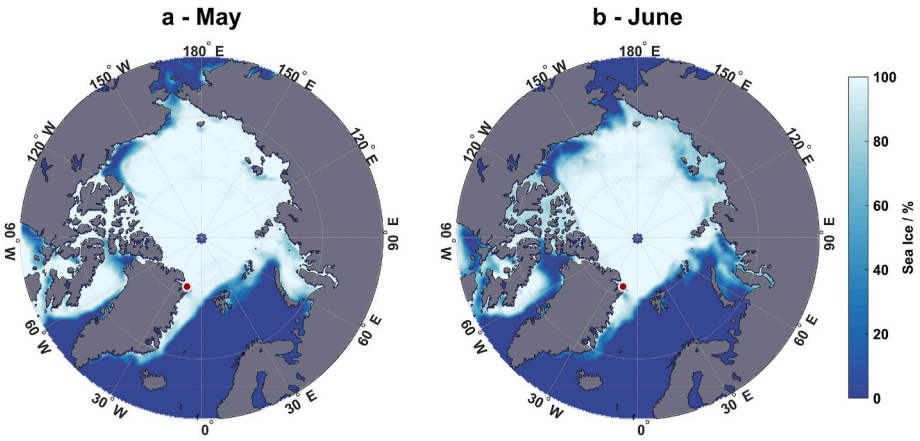

Fig. 5. Sea Ice coverages around Greenland in a) May and b) June 2016.

assemblages in the respective source regions. For example, Becagli et al. (2016) calculated similar slopes for MSA at Thule with primary production in Baffin Bay and MSA at Ny-Ålesund with primary production in the Barents Sea. However, the slope between MSA at Ny-Ålesund and primary production in the Greenland Sea was significantly lower. This finding indicates a similar atmospheric yield of MSA for a similar amount of primary production in the two seas. This explanation is reasonable for the similar levels of the MOA factor and MSA observed when source regions shifted from the east (the Barents Sea and Greenland Sea in May) to the west (Baffin Bay and Canadian Arctic Archipelago in June). This relationship supports the findings of Collins et al. (2017) that marine biological processes play a key role in regulating the atmospheric load of aerosol particles.

4. Conclusion

The non-refractory mass of PM_1 (NR-PM_1) calculated from the measured sum of organic species, SO_4^{2-}, NO_3^-, NH_4^+ and Cl averaged 0.57 μg m^{-3} over the campaign from May–June 2016. SO_4^{2-} was the major component accounting for 48% followed by organics (40%). While NR-PM_1 loading was similar from May–June, SO_4^{2-} decreased from 0.35 to 0.19 μg m^{-3} in June. Conversely, organics increased from 0.18 to 0.30 μg m^{-3}. By use of Positive Matrix Factorization using SoFi, a hydrocarbon-like organic aerosol factor (HOA), an oxygenated organic aerosol factor (OOA) and a marine organic aerosol factor (MOA) were found to contribute by 5%, 77% and 18% to the organic aerosol (OA). The largest contribution to OA was from OOA, which was dominated *by m/z* 44 (and 28) and otherwise showing only little fragmentation, which indicates that this factor is highly oxidized. OOA correlated with accumulation mode particles and atmospheric SO_4^{2-}, which indicated anthropogenic oxidized organic aerosols predominantly from long-range transport during winter and spring at Villum. The MOA factor was characterized by mass spectral fragments of methane sulfonic acid (MSA). Since MSA is formed during atmospheric oxidation of dimethyl sulfide, the MOA factor is considered biogenic in origin. MOA correlated with Aitken mode particle mass. This indicates that biogenic processes are not only a significant source of aerosols at Villum and in the High Arctic, but MOA also appears to be formed on a regional scale in the Arctic, since Aitken mode particles are generally not long-range transported due to their short atmospheric lifetime.

During May, air masses frequently arrived from the east (the Barents Sea and Greenland Sea), although the source regions for the MOA factor and MSA were located in the Barents Sea and Lincoln Sea with lesser contributions from the Greenland Sea. During June, air masses shifted to arrive from the west (Baffin Bay and the Canadian Arctic Archipelago) and the source regions for the MOA factor and MSA shifted correspondingly. During May, marginal sea ice zones were present in the Barents Sea between Svalbard and Franz Josef Land, while during June, sea ice in the northern part of Baffin Bay retreated and sea ice in the Canadian Arctic Archipelago decreased. Although May and June experienced different transport patterns and sea ice conditions, levels of the MOA factor and MSA were similar between months. This is likely due to similarities between marine biological activities in the Barents Sea and Baffin Bay. This research highlights the complex relationship between transport patterns, sea ice conditions, and atmospheric particulate sulfur concentrations, however multiyear aerosol chemical composition from several High Arctic sites is needed to determine the full effects of ocean-atmosphere interactions and transport patterns on atmospheric aerosol concentrations.

Financial support

This research has been financially supported by the Danish Environmental Protection Agency and the Danish Energy Agency, with means from MIKA/DANCEA funds for environmental support to the Arctic region (project nos. Danish EPA: MST-113-00-140; Ministry of Climate, Energy, and Utilities: 2018-3767) and ERA-PLANET (The European Network for observing our changing Planet) projects, as well as by iGOSP, iCUPE.

CRediT authorship contribution statement

J.K. Nøjgaard: Conceptualization, Methodology, Formal analysis, Writing – original draft, Writing – review & editing, Supervision. **L. Peker:** Conceptualization, Methodology, Formal analysis, Writing – original draft, Writing – review & editing. **J.B. Pernov:** Conceptualization, Methodology, Writing – original draft, Formal analysis, Writing – review & editing. **M.S. Johnson:** Writing – review & editing. **R. Bossi:** Writing – review & editing. **A. Massling:** Formal analysis, Writing – review & editing. **R. Lange:** Software, Validation, Writing – review & editing. **I.E. Nielsen:** Writing – review & editing. **A.S.H. Prevot:** Validation, Writing – review & editing. **A.C. Eriksson:** Validation, Writing – review & editing. **F. Canonaco:** Software, Validation, Writing – review & editing. **H. Skov:** Methodology, Formal analysis, Investigation, Writing – review & editing, Funding acquisition, Supervision.

Declaration of competing interest

The authors declare that they have no known competing financial interests or personal relationships that could have appeared to influence the work reported in this paper.

Acknowledgements

The Villum Foundation is gratefully acknowledged for financing the establishment of the Villum Research Station and the instrumentation used in this study (ACSM). Thanks to the Royal Danish Air Force and the Arctic Command for providing logistic support to the project. Christel Christoffersen, Bjarne Jensen, and Keld Mortensen are gratefully acknowledged for their technical support.

Appendix A. Supplementary data

Supplementary data to this article can be found online at https://doi.org/10.1016/j.atmosenv.2022.119241.

References

Aiken, A.C., Salcedo, D., Cubison, M.J., Huffman, J.A., DeCarlo, P.F., Ulbrich, I.M., Docherty, K.S., Sueper, D., Kimmel, J.R., Worsnop, D.R., Trimborn, A., Northway, M., Stone, E.A., Schauer, J.J., Volkamer, R.M., Fortner, E., de Foy, B., Wang, J., Laskin, A., Shutthanandan, V., Zheng, J., Zhang, R., Gaffney, J., Marley, N. A., Paredes-Miranda, G., Arnott, W.P., Molina, L.T., Sosa, G., Jimenez, J.L., 2009. Mexico City aerosol analysis during MILAGRO using high resolution aerosol mass spectrometry at the urban supersite (T0) – Part 1: fine particle composition and organic source apportionment. Atmos. Chem. Phys. 9, 6633–6653. https://doi.org/10.5194/acp-9-6633-2009.

Allan, J.D., Delia, A.E., Coe, H., Bower, K.N., Alfarra, M.R., Jimenez, J.L., Middlebrook, A.M., Drewnick, F., Onasch, T.B., Canagaratna, M.R., Jayne, J.T., Worsnop, D.R., 2004. A generalised method for the extraction of chemically resolved mass spectra from Aerodyne aerosol mass spectrometer data. J. Aerosol Sci. 35, 909–922. https://doi.org/10.1016/j.jaerosci.2004.02.007, 2004.

AMAP, 2011. In: Quinn, P.K., Stohl, A., Arneth, A., Berntsen, T., Burkhart, J.F., Christensen, J., Flanner, M., Kupiainen, K., Lihavainen, H., Shepherd, M., Shevchenko, V., Skov, H., Vestreng, V. (Eds.), The Impact of Black Carbon on Arctic Climate (2011), AMAP Technical Report No. 4 (2011), Arctic Monitoring and Assessment Programme (AMAP), vol. 72, p. 2011. Oslo.

Ashbaugh, L.L., Malm, W.C., Sadeh, W.Z., 1985. A residence time probability analysis of sulfur concentrations at grand Canyon National Park. Atmos. Environ. 19, 1263–1270. https://doi.org/10.1016/0004-6981(85)90256-2, 1967.

Avery, A.M., Waring, M.S., DeCarlo, P.F., 2019. Seasonal variation in aerosol composition and concentration upon transport from the outdoor to indoor environment. Environ. Sci.: Process. Impacts 20, 528–547.

Baccarini, A., Dommen, J., Lehtipalo, K., Henning, S., Modini, R.L., Gysel-Beer, M., Baltensperger, U., Schmale, J., 2021. Low-volatility vapors and new particle formation over the southern ocean during the Antarctic circumnavigation expedition. J. Geophys. Res. Atmos. 126, e2021JD035126 https://doi.org/10.1029/2021JD035126.

Barrett, T.E., Robinson, E.M., Usenko, S., Sheesley, R.J., 2015. Source contributions to wintertime elemental and organic carbon in the western Arctic based on radiocarbon and tracer apportionment. Environ. Sci. Technol. 49 https://doi.org/10.1021/acs.est.5b05128, 13733–13733.

Barrie, L.A., Hoff, R.M., Daggupaty, S.M., 1981. The influence of mid-latitudinal pollution sources on haze in the Canadian Arctic. Atmos. Environ. 15 (8), 1407–1419, 1967.

Becagli, S., Lazzara, L., Fani, F., Marchese, C., Traversi, R., Severi, M., di Sarra, A., Sferlazzo, D., Piacentino, S., Bom- marito, C., Dayan, U., Udisti, R., 2013. Relationship between methanesulfonate (MS-) in atmospheric particulate and remotely sensed phytoplankton activity in oligo-mesotrophic central Mediterranean Sea. Atmos. Environ. 79, 681–688. https://doi.org/10.1016/j.atmosenv.2013.07.032.

Becagli, S., Lazzara, L., Marchese, C., Dayan, U., Ascanius, S.E., Cacciani, M., Caiazzo, L., Di Biagio, C., Di Iorio, T., di Sarra, A., Eriksen, P., Fani, F., Giardi, F., Meloni, D., Muscari, G., Pace, G., Severi, M., Traversi, R., Udisti, R., 2016. Relationships linking primary production, sea ice melting, and biogenic aerosol in the Arctic. Atmos. Environ. 136, 1–15.

Becagli, S., Amore, A., Caiazzo, L., Iorio, T.D., Sarra, A.D., Lazzara, L., Marchese, C., Meloni, D., Mori, G., Muscari, G., Nuccio, C., Pace, G., Severi, M., Traversi, R., 2019. Biogenic aerosol in the Arctic from eight years of MSA data from Ny Ålesund (Svalbard Islands) and Thule (Greenland). Atmosphere 10, 349. https://doi.org/10.3390/atmos10070349.

Beck, L.J., Sarnela, N., Junninen, H., Hoppe, C.J.M., Garmash, O., Bianchi, F., Riva, M., Rose, C., Perakyla, O., Wimmer, D., Kausiala, O., Jokinen, T., Ahonen, L., Mikkila, J., Hakala, J., He, X.C., Kontkanen, J., Wolf, K.K.E., Cappelletti, D., Mazzola, M., Traversi, R., Petroselli, C., Viola, A.P., Vitale, V., Lange, R., Massling, A., Nojgaard, J. K., Krejci, R., Karlsson, L., Zieger, P., Jang, S., Lee, K., Vakkari, V., Lampilahti, J., Thakur, R.C., Leino, K., Kangasluoma, J., Duplissy, E.M., Siivola, E., Marbouti, M., Tham, Y.J., Saiz-Lopez, A., Petaja, T., Ehn, M., Worsnop, D.R., Skov, H., Kulmala, M., Kerminen, V.M., Sipila, M., 2021. Differing mechanisms of new particle formation at two Arctic sites. Geophys. Res. Lett. 48, e2020GL091334 https://doi.org/10.1029/2020GL091334.

Birch, M., 1998. Analysis of carbonaceous aerosols: interlaboratory comparison. Analyst 123 (5), 851–857.

Bozem, H., Hoor, P., Kunkel, D., Kollner, F., Schneider, J., Herber, A., Schulz, H., Leaitch, W.R., Aliabadi, A.A., Willis, M., Burkart, J., Abbatt, J., 2019. Characterization of transport regimes and the polar dome during Arctic spring and summer using in situ aircraft measurements. Atmos. Chem. Phys. 19 (23), 15049–15071.

Brock, C.A., Cozic, J., Bahreini, R., Froyd, K.D., Middlebrook, A.M., McComiskey, A., Brioude, J., Cooper, O.R., Stohl, A., Aikin, K.C., de Gouw, J.A., Fahey, D.W., Ferrare, R.A., Gao, R.-S., Gore, W., Holloway, J.S., Hübler, G., Jefferson, A., Lack, D. A., Lance, S., Moore, R.H., Murphy, D.M., Nenes, A., Novelli, P.C., Nowak, J.B., Ogren, J.A., Peischl, J., Pierce, R.B., Pilewskie, P., Quinn, P.K., Ryerson, T.B., Schmidt, K.S., Schwarz, J.P., Sodemann, H., Spackman, J.R., Stark, H., Thomson, D. S., Thornberry, T., Veres, P., Watts, L.A., Warneke, C., Wollny, A.G., 2011. Characteristics, sources, and transport of aerosols measured in spring 2008 during the aerosol, radiation, and cloud processes affecting Arctic Climate (ARCPAC) Project. Atmos. Chem. Phys. 11, 2423–2453. https://doi.org/10.5194/acp-11-2423-2011.

Budisulistiorini, S.H., Canagaratna, M.R., Croteau, P.L., Marth, W.J., Baumann, K., Edgerton, E.S., Shaw, S.L., Knipping, E.M., Worsnop, D.R., Jayne, J.T., Gold, A., Surratt, J.D., 2013. Real-Time continuous characterization of secondary organic aerosol derived from isoprene epoxydiols in downtown Atlanta, Georgia using the Aerodyne Aerosol Chemical Speciation Monitor. Environ. Sci. Technol. 47, 5686–5694.

Canagaratna, M.R., Jayne, J.T., Jimenez, J.L., Allan, J.D., Alfarra, M.R., Zhang, Q., Onasch, T.B., Drewnick, F., Coe, H., Middlebrook, A., Delia, A., Williams, L.R., Trimborn, A.M., Northway, M.J., DeCarlo, P.F., Kolb, C.E., Davidovits, P., Worsnop, D.R., 2007. Chemical and microphysical characterization of ambient aerosols with the aerodyne aerosol mass spectrometer. Mass Spectrom. Rev. 26, 185–222. https://doi.org/10.1002/mas.20115.

Canonaco, F., Crippa, M., Slowik, J.G., Baltensperger, U., Prevot, A.S.H., 2013. SoFi, an IGOR-based interface for the efficient use of the generalized multilinear engine (ME-2) for the source apportionment: ME-2 application to aerosol mass spectrometer data. Atmos. Meas. Tech. 6, 3649–3661.

Carpenter, L.J., Archer, S.D., Beale, R., 2012. Ocean-atmosphere trace gas exchange. Chem. Soc. Rev. 41 (19), 6473–6506. https://doi.org/10.1039/c2cs35121h.

Carslaw, D.C., Ropkins, K., 2012. Openair — an R package for air quality data analysis. Environ. Model. Software 27–28, 52–61. https://doi.org/10.1016/j.envsoft.2011.09.008, 2012.

Cavalli, F., Viana, M., Yttri, K.E., Genberg, J., Putaud, J.-P., 2010. Toward a standardised thermal-optical protocol for measuring atmospheric organic and elemental carbon: the EUSAAR protocol. Atmos. Meas. Tech. 3, 79–89. https://doi.org/10.5194/amt-3-79-2010.

Chang, R.Y.-W., Leck, C., Graus, M., Müller, M., Paatero, J., Burkhart, J.F., Stohl, A., Orr, L.H., Hayden, K., Li, S.-M., Hansel, A., Tjernström, M., Leaitch, W.R., Abbatt, J. P.D., 2011. Aerosol composition and sources in the central Arctic Ocean during ASCOS. Atmos. Chem. Phys. 11, 10619–10636. https://doi.org/10.5194/acp-11-10619-2011.

Chen, Q., Sherwen, T., Evans, M., Alexander, B., 2018. DMS oxidation and sulfur aerosol formation in the marine troposphere: a focus on reactive halogen and multiphase chemistry. Atmos. Chem. Phys. 18 (18), 13617–13637. https://doi.org/10.5194/acp-18-13617-2018.

Collins, D.B., Burkart, J., Chang, R.Y.-W., Lizotte, M., Boivin-Rioux, A., Blais, M., Mungall, E.L., Boyer, M., Irish, V.E., Massé, G., Kunkel, D., Tremblay, J.-É., Papakyriakou, T., Bertram, A.K., Bozem, H., Gosselin, M., Levasseur, M., Abbatt, J.P. D., 2017. Frequent ultrafine particle formation and growth in Canadian Arctic marine and coastal environments. Atmos. Chem. Phys. 17, 13119–13138. https://doi.org/10.5194/acp-17-13119-2017.

Crippa, M., Canonaco, F., Lanz, V.A., Aijala, M., Allan, J.D., Carbone, S., Capes, G., Ceburnis, D., Dall'Osto, M., Day, D.A., DeCarlo, P.F., Ehn, M., Eriksson, A., Freney, E., Ruiz, L.H., Hillamo, R., Jimenez, J.L., Junninen, H., Kiendler-Scharr, A., Kortelainen, A.M., Kulmala, M., Laaksonen, A., Mensah, A., Mohr, C., Nemitz, E., O'Dowd, C., Ovadnevaite, J., Pandis, S.N., Petaja, T., Poulain, L., Saarikoski, S., Sellegri, K., Swietlicki, E., Tiitta, P., Worsnop, D.R., Baltensperger, U., Prevot, A.S.H., 2014. Organic aerosol components derived from 25 AMS data sets across Europe using a consistent ME-2 based source apportionment approach. Atmos. Chem. Phys. 14, 6159–6176.

Dall'Osto, M., Geels, C., Beddows, D.C.S., Boertmann, D., Lange, R., Nøjgaard, J.K., Harrison, R., Simo, R., Skov, H., Massling, A., 2018a. Regions of open water and melting sea ice drive new particle formation in North East Greenland. Sci. Rep. 8, 6109. https://doi.org/10.1038/s41598-018-24426-8, 2018.

Dall'Osto, M., Simo, R., Harrison, R.M., Beddows, D.C.S., Saiz-Lopez, A., Lange, R., Skov, H., Nøjgaard, J.K., Nielsen, I.E., Massling, A., 2018b. Abiotic and biotic sources influencing spring new particle formation in North East Greenland. Atmos. Environ. 190, 126–134.

Draxler, R.R., Hess, G.D., 1998. An overview of the HYSPLIT_4 modelling system for trajectories, dispersion and deposition. Aust. Meteorol. Mag. 47, 295–308.

Duplissy, J., DeCarlo, P.F., Dommen, J., Alfarra, M.R., Metzger, A., Barmpadimos, I., Prevot, A.S.H., Weingartner, E., Tritscher, T., Gysel, M., Aiken, A.C., Jimenez, J.L., Canagaratna, M.R., Worsnop, D.R., Collins, D.R., Tomlinson, J., Baltensperger, U., 2011. Relating hygroscopicity and composition of organic aerosol particulate matter. Atmos. Chem. Phys. 11, 1155–1165. https://doi.org/10.5194/acp-11-1155-2011.

Fan, J., Wang, Y., Rosenfeld, D., Liu, X., 2016. Review of aerosol–cloud interactions: mechanisms, significance, and challenges. J. Atmos. Sci. 73, 4221–4252.

Fenger, M., Sørensen, L.L., Kristensen, K., Jensen, B., Nguyen, Q.T., Nøjgaard, J.K., Massling, A., Skov, H., Becker, T., Glasius, M., 2013. Sources of anions in aerosols in northeast Greenland during late winter. Atmos. Chem. Phys. 13, 1569–1578. https://doi.org/10.5194/acp-13-1569-2013.

Fröhlich, R., Cubison, M.J., Slowik, J.G., Bukowiecki, N., Canonaco, F., Croteau, P.L., Gysel, M., Henne, S., Herrmann, E., Jayne, J.T., Steinbacher, M., Worsnop, D.R., Baltensperger, U., Prévôt, A.S.H., 2015. Fourteen months of on-line measurements of the non-refractory submicron aerosol at the Jungfraujoch (3580 m a.s.l.) – chemical composition, origins and organic aerosol sources. Atmos. Chem. Phys. 15, 11373–11398. https://doi.org/10.5194/acp-15-11373-2015.

Fröhlich, R., Cubison, M.J., Slowik, J.G., Bukowiecki, N., Prévôt, A.S.H., Baltensperger, U., Schneider, J., Kimmel, J.R., Gonin, M., Rohner, U., Worsnop, D.R., Jayne, J.T., 2013. The ToF-ACSM: a portable aerosol chemical speciation monitor with TOFMS detection. Atmos. Meas. Tech. 6, 3225–3241. https://doi.org/10.5194/amt-6-3225-2013.

Frossard, A.A., Shaw, P.M., Russell, L.M., Kroll, J.H., Canagaratna, M.R., Worsnop, D.R., Quinn, P.K., Bates, T.S., 2011. Springtime Arctic haze contributions of submicron organic particles from European and Asian combustion sources. J. Geophys. Res. 116, D05205 https://doi.org/10.1029/2010JD015178.

Galí, M., Simó, R., 2010. Occurrence and cycling of dimethylated sulfur compounds in the Arctic during summer receding of the ice edge. Mar. Chem. 122, 105–117. https://doi.org/10.1016/j.marchem.2010.07.003.

Guo, J., Zhou, S., Cai, M., Zhao, J., Song, W., Zhao, W., Hu, W., Sun, Y., He, Y., Yang, C., Xu, X., Zhang, Z., Cheng, P., Fan, Q., Hang, J., Fan, S., Wang, X., Wang, X., 2020. Characterization of submicron particles by time-of-flight aerosol chemical speciation monitor (ToF-ACSM) during wintertime: aerosol composition, sources, and chemical processes in Guangzhou, China. Atmos. Chem. Phys. 20, 7595–7615. https://doi.org/10.5194/acp-20-7595-2020.

Heidam, N.Z., 1984. The components of the Arctic aerosol. Atmos. Environ. 18 (2), 329–343, 1967.

Heidam, N.Z., Wahlin, P., Christensen, J.H., 1999. Tropospheric gases and aerosols in Northeast Greenland. J. Atmos. Sci. 56, 261–278. https://doi.org/10.1175/1520-0469(1999)056<0261:TGAAIN>2.0.CO;2.

Heidam, N.Z., Christensen, J., Wåhlin, P., Skov, H., 2004. Arctic atmospheric contaminants in NE Greenland: levels, variations, origins, transport, transformations and trends 1990–2001. Sci. Total Environ. 331, 5–28. https://doi.org/10.1016/j.scitotenv.2004.03.033.

Heintzenberg, J., Leck, C., 1994. Seasonal variation of the atmospheric aerosol near the top of the marine boundary layer over Spitsbergen related to the Arctic sulphur cycle. Tellus B 46 (1), 52–67.

Hirdman, D., Sodemann, H., Eckhardt, S., Burkhart, J.F., Jefferson, A., Mefford, T., Quinn, P.K., Sharma, S., Ström, J., Stohl, A., 2010. Source identification of short-lived air pollutants in the Arctic using statistical analysis of measurement data and particle dispersion model output. Atmos. Chem. Phys. 10, 669–693. https://doi.org/10.5194/acp-10-669-2010.

Hoffmann, E.H., Tilgner, A., Schrödner, R., Bräuer, P., Wolke, R., Herrmann, H., 2016. An advanced modeling study on the impacts and atmospheric implications of multiphase dimethyl sulfide chemistry. Proc. Natl. Acad. Sci. U.S.A. 113 (42), 11776–11781. https://doi.org/10.1073/pnas.1606320113.

Huang, S., Poulain, L., van Pinxteren, D., van Pinxteren, M., Wu, Z.J., Herrmann, H., Wiedensohler, A., 2017. Latitudinal and seasonal distribution of particulate MSA over the Atlantic using a Vali- dated quantification method with HR-ToF-AMS. Environ. Sci. Technol. 51, 418–426. https://doi.org/10.1021/acs.est.6b03186.

IPCC, 2013. Climate Change 2013: the Physical Science Basis. Contribution of Working Group I to the Fifth Assessment Report of the Intergovernmental Panel on Climate Change. Cambridge University Press, Cambridge, United Kingdom and New York, NY, USA, p. 1535, 2013.

IPCC, 2021. In: Zhai, V.P., Pirani, A., Connors, S.L., Péan, C., Berger, S., Caud, N., Chen, Y., Goldfarb, L., Gomis, M.I., Huang, M., Leitzell, K., Lonnoy, E., Matthews, J. B.R., Maycock, T.K., Waterfield, T., Yelekçi, O., Yu, R., Zhou, B. (Eds.), Climate Change 2021: The Physical Science Basis. Contribution of Working Group I to the Sixth Assessment Report of the Intergovernmental Panel on Climate Change [Masson-Delmotte. Cambridge University Press (in press).

Jimenez, J.L., Canagaratna, M.R., Donahue, N.M., Prevot, A.S.H., Zhang, Q., Kroll, J.H., DeCarlo, P.F., Allan, J.D., Coe, H., Ng, N.L., Aiken, A.C., Docherty, K.S., Ulbrich, I. M., Grieshop, A.P., Robinson, A.L., Duplissy, J., Smith, J.D., Wil- son, K.R., Lanz, V. A., Hueglin, C., Sun, Y.L., Tian, J., Laak- sonen, A., Raatikainen, T., Rautiainen, J., Vaattovaara, P., Ehn, M., Kulmala, M., Tomlinson, J.M., Collins, D.R., Cubison, M.J., Dunlea, E.J., Huffman, J.A., Onasch, T.B., Alfarra, M.R., Williams, P.I., Bower, K., Kondo, Y., Schneider, J., Drewnick, F., Borrmann, S., Weimer, S., Demerjian, K., Salcedo, D., Cot- trell, L., Griffin, R., Takami, A., Miyoshi, T., Hatakeyama, S., Shimono, A., Sun, J.Y., Zhang, Y.M., Dzepina, K., Kimmel, J.R., Sueper, D., Jayne, J. T., Herndon, S.C., Trimborn, A.M., Williams, L.R., Wood, E.C., Middlebrook, A.M., Kolb, C.E., Baltensperger, U., Worsnop, D.R., 2009. Evolution of organic aerosols in the atmosphere. Science 326, 1525–1529. https://doi.org/10.1126/science.1180353.

Karl, M., Leck, C., Coz, E., Heintzenberg, J., 2013. Marine nanogels as a source of atmospheric nanoparticles in the high Arctic. Geophys. Res. Lett. 40, 3738–3743. https://doi.org/10.1002/grl.50661.

Kawamura, K., Kasukabe, H., Barrie, L.A., 2010. Secondary formation of water-soluble organic acids and alpha-dicarbonyls and their contributions to total carbon and water-soluble organic carbon: photochemical aging of organic aerosols in the Arctic spring. J. Geophys. Res. Atmos. 115, D21306 https://doi.org/10.1029/2010jd014299.

Lange, R., Dall'Osto, M., Skov, H., Nøjgaard, J.K., Nielsen, I.E., Beddows, D.C.S., Simo, R., Harrison, R.M., Massling, A., 2018. Characterization of distinct Arctic aerosol accumulation modes and their sources. Atmos. Environ. 183, 1–10.

Leaitch, W.R., Russell, L.M., Liu, J., Kolonjari, F., Toom, D., Huang, L., Sharma, S., Chivulescu, A., Veber, D., Zhang, W., 2018. Organic functional groups in the submicron aerosol at 82.5◦ N, 62.5◦ W from 2012 to 2014. Atmos. Chem. Phys. 18, 3269–3287. https://doi.org/10.5194/acp-18-3269-2018.

Leck, C., Bigg, E.K., 2005. Source and evolution of the marine aerosol – a new perspective. Geophys. Res. Lett. 32, L19803 https://doi.org/10.1029/2005gl023651.

Leck, C., Persson, C., 1996. The central Arctic Ocean as a source of dimethyl sulfide: seasonal variability in relation to biological activity. Tellus B 48, 156–177.

Lee, H., Lee, K., Lunder, C.R., Krejci, R., Aas, W., Park, J., Park, K.T., Lee, B.Y., Yoon, Y.J., Park, K., 2020. Atmospheric new particle formation characteristics in the Arctic as measured at Mount Zeppelin, Svalbard, from 2016 to 2018. Atmos. Chem. Phys. 20, 13425–13441. https://doi.org/10.5194/acp-20-13425-2020.

Lenssen, N.J.L., Schmidt, G.A., Hansen, J.E., Menne, M.J., Persin, A., Ruedy, R., Zyss, D., 2019. Improvements in the GISTEMP uncertainty model. J. Geophys. Res. Atmos. 124, 6307–6326. https://doi.org/10.1029/2018JD029522.

Lenton, T.M., 2012. Arctic climate tipping points. Ambio 41 (1), 10–22.

Lenton, T.M., Rockström, J., Gaffney, O., Ramstorf, S., Richardson, K., Steffen, W., Schnellnhuber, H.J., 2019. Climate Tipping Points – too risky to bet against. Nature 575 (7784), 592–595.

Liu, P.S.K., Deng, R., Smith, K.A., Williams, L.R., Jayne, J.T., Canagaratna, M.R., Moore, K., Onasch, T.B., Worsnop, D.R., Deshler, T., 2007. Transmission efficiency of an aerodynamic focusing lens system: comparison of model calculations and laboratory measurements for the aerodyne aerosol mass spectrometer. Aerosol. Sci. Technol. 41, 721–733.

Matrai, P., Vernet, M., Wassmann, P., 2007. Relating temporal and spatial patterns of DMSP in the Barents Sea to phytoplankton biomass and productivity. J. Mar. Syst. 67, 83–101. https://doi.org/10.1016/j.jmarsys.2006.10.001.

Matthew, B.M., Middlebrook, A.M., Onasch, T.B., 2008. Collection efficiencies in an Aerodyne Aerosol Mass Spectrometer as a function of particle phase for laboratory generated aerosols. Aerosol. Sci. Technol. 42, 884–898. https://doi.org/10.1080/02786820802356797.

Middlebrook, A.M., Bahreini, R., Jimenez, J.L., Canagaratna, M.R., 2012. Evaluation of composition-dependent collection efficiencies for the aerodyne aerosol mass spectrometer using field data. Aerosol. Sci. Technol. 46, 258–271. https://doi.org/10.1080/02786826.2011.620041.

Ng, N.L., Herndon, S.C., Trimborn, A., Canagaratna, M.R., Croteau, P.L., Onasch, T.B., Sueper, D., Worsnop, D.R., Zhang, Q., Sun, Y.L., Jayne, J.T., 2011. An aerosol chemical speciation monitor (ACSM) for routine monitoring of the composition and mass concentrations of ambient aerosol. Aerosol. Sci. Technol. 45 (7), 780–794. https://doi.org/10.1080/02786826.2011.560211.

Nguyen, Q.T., Skov, H., Sorensen, L.L., Jensen, B.J., Grube, A.G., Massling, A., Glasius, M., Nojgaard, J.K., 2013. Source apportionment of particles at station Nord, North east Greenland during 2008-2010 using COPREM and PMF analysis. Atmos. Chem. Phys. 13 (1), 35–49.

Nguyen, Q.T., Glasius, M., Sørensen, L.L., Jensen, B., Skov, H., Birmili, W., Wiedensohler, A., Kristensson, A., Nøjgaard, J.K., Massling, A., 2016. Seasonal variation of atmospheric particle number concentrations, new particle formation and atmospheric oxidation capacity at the high Arctic site Villum Research Station, Station Nord. Atmos. Chem. Phys. 16, 11319–11336. https://doi.org/10.5194/acp-16-11319-2016.

Nielsen, I.E., Skov, H., Massling, A., Eriksson, A.C., Dall'Osto, M., Junninen, H., Sarnela, N., Lange, R., Collier, S., Zhang, Q., Cappa, C.D., Nøjgaard, J.K., 2019. Biogenic and anthropogenic sources of Arctic aerosols. Atmos. Chem. Phys. 19, 10239–10256.

Orellana, M.V., Matrai, P.A., Leck, C., Rauschenberg, C.D., Lee, A.M., Coz, E., 2011. Marine microgels as a source of cloud condensation nuclei in the high Arctic. Proc. Natl. Acad. Sci. USA 108, 13612–13617. https://doi.org/10.1073/pnas.1102457108.

Paatero, P., Tapper, U., 1994. Positive matrix factorization – a nonnegative factor model with optimal utilization of error-estimates of data values. Environmetrics 5, 111–126. https://doi.org/10.1002/env.3170050203.

Park, K.-T., Lee, K., Kim, T.-W., Yoon, Y.J., Jang, E.-H., Jang, S., Lee, B.-Y., Hermansen, O., 2018. Atmospheric DMS in the Arctic Ocean and its relation to phytoplankton biomass. Global Biogeochem. Cycles 32, 351–359. https://doi.org/10.1002/2017GB005805.

Pernov, J.B., Bossi, R., Lebourgeois, T., Nojgaard, J.K., Holzinger, R., Hjorth, J.L., Skov, H., 2021. Atmospheric VOC measurements at a High Arctic site: characteristics and source apportionment. Atmos. Chem. Phys. 21, 2895–2916. https://doi.org/10.5194/acp-21-2895-2021.

Perrette, M., Yool, A., Quartly, G.D., Popova, E.E., 2011. Near-ubiquity of ice-edge blooms in the Arctic. Biogeosciences 8, 515–524. https://doi.org/10.5194/bg-8-515-2011.

Quinn, P.K., Miller, T.L., Bates, T.S., Ogren, J.A., Andrews, E., Shaw, G.E., 2002. A 3-year record of simultaneously measured aerosol chemical and optical properties at Barrow, Alaska. J. Geophys. Res. Atmos. 107, 4130. https://doi.org/10.1029/2001jd001248.

Quinn, P., Shaw, G., Andrews, E., Dutton, E.G., Ruoho-Airola, T., Gong, S.L., 2007. Arctic haze: current trends and knowledge gaps. Tellus B 59 (1), 99–114.

Rattanavaraha, W., Canagaratna, M.R., Budisulistiorini, S.H., Croteau, P.L., Baumann, K., Canonaco, F., Prevot, A.S.H., Edgerton, E.S., Zhang, Z., Jayne, J.T., Worsnop, D.R., Gold, A., Shaw, S.L., Surratt, J.D., 2017. Source apportionment of submicron organic aerosol collected from Atlanta, Georgia, during 2014–2015 using the aerosol chemical speciation monitor (ACSM). Atmos. Environ. 167, 389–402.

Regayre, L.A., Schmale, J., Johnson, J.S., Tatzelt, C., Baccarini, A., Henning, S., Yoshioka, M., Stratmann, F., Gysel-Beer, M., Grosvenor, D.P., Carslaw, K.S., 2020. The value of remote marine aerosol measurements for constraining radiative forcing

uncertainty. Atmos. Chem. Phys. 20, 10063–10072. https://doi.org/10.5194/acp-20-10063-2020.

Ripoll, A., Minguillón, M.C., Pey, J., Jimenez, J.L., Day, D.A., Sosedova, Y., Canonaco, F., Prévôt, A.S.H., Querol, X., Alastuey, A., 2015. Long-term real-time chemical characterization of submicron aerosols at Montsec (southern Pyrenees, 1570 m a.s.l.). Atmos. Chem. Phys. 15, 2935–2951. https://doi.org/10.5194/acp-15-2935-2015.

Rolph, G., Stein, A., Stunder, B., 2017. Real-time environmental applications and display sYstem: READY. Environ. Model. Software 95, 210–228. https://doi.org/10.1016/j.envsoft.2017.06.025.

Schlag, P., Kiendler-Scharr, A., Blom, M.J., Canonaco, F., Henzing, J.S., Moerman, M., Prévôt, A.S.H., Holzinger, R., 2016. Aerosol source apportionment from 1-year measurements at the CESAR tower in Cabauw, The Netherlands. Atmos. Chem. Phys. 16, 8831–8847. https://doi.org/10.5194/acp-16-8831-2016.

Shaw, P.M., Russell, L.M., Jefferson, A., Quinn, P.K., 2010. Arctic organic aerosol measurements show particles from mixed combustion in spring haze and from frost flowers in winter. Geophys. Res. Lett. 37, L10803 https://doi.org/10.1029/2010gl042831.

Sipila, M., Sarnela, N., Jokinen, T., Henschel, H., Junninen, H., Kontkanen, J., Richters, S., Kangasluoma, J., Franchin, A., Perakyla, O., Rissanen, M.P., Ehn, M., Vehkamaki, H., Kurten, T., Berndt, T., Petaja, T., Worsnop, D., Ceburnis, D., Kerminen, V.M., Kulmala, M., O'Dowd, C., 2016. Molecular-scale evidence of aerosol particle formation via sequential addition of HIO3. Nature 537 (7621), 532–534, 2016.

Skov, H., Wahlin, P., Christensen, J., Heidam, N.Z., Petersen, D., 2006. Measurements of elements, sulphate and SO_2 in Nuuk Greenland. Atmos. Environ. 40 (25), 4775–4781.

Sodemann, H., Pommier, M., Arnold, S.R., Monks, S.A., Stebel, K., Burkhart, J.F., Hair, J.W., Diskin, G.S., Clerbaux, C., Coheur, P.-F., Hurtmans, D., Schlager, H., Blechschmidt, A.-M., Kristjánsson, J.E., Stohl, A., 2011. Episodes of cross-polar transport in the Arctic troposphere during July 2008 as seen from models, satellite, and aircraft observations. Atmos. Chem. Phys. 11, 3631–3651. https://doi.org/10.5194/acp-11-3631-2011.

Stohl, A., 2006. Characteristics of atmospheric transport into the Arctic troposphere. J. Geophys. Res., [Atmos.] 111, D11306. https://doi.org/10.1029/2005jd006888.

Stroeve, J., Holland, M.M., Meier, W., Scambos, T., Serreze, M., 2007. Arctic sea ice decline: faster than forecast. Geophys. Res. Lett. 34, L09501 https://doi.org/10.1029/2007gl029703.

Timonen, H., Cubison, M., Aurela, M., Brus, D., Lihavainen, H., Hillamo, R., Canagaratna, M., Nekat, B., Weller, R., Worsnop, D., Saarikoski, S., 2016. Applications and limitations of constrained high-resolution peak fitting on low resolving power mass spectra from the ToF-ACSM. Atmos. Meas. Tech. 9, 3263–3281. https://doi.org/10.5194/amt-9-3263-2016.

Tunved, P., Ström, J., Krejci, R., 2013. Arctic aerosol life cycle: linking aerosol size distributions observed between 2000 and 2010 with air mass transport and precipitation at Zeppelin station, Ny-Ålesund, Svalbard. Atmos. Chem. Phys. 13 (7), 3643–3660.

Turpin, B.J., Lim, H.-J., 2001. Species contributions to $PM_{2.5}$ mass concentrations: revisiting common assumptions for estimating organic mass. Aerosol. Sci. Technol. 35 (1), 602–610.

Twomey, S., 1977. The influence of pollution on the shortwave albedo of clouds. J. Atmos. Sci. 34 (7), 1149–1152.

Ulbrich, I.M., Canagaratna, M.R., Zhang, Q., Worsnop, D.R., Jimenez, J.L., 2009. Interpretation of organic components from positive matrix factorization of aerosol mass spectrometric data. Atmos. Chem. Phys. 9, 2891–2918. https://doi.org/10.5194/acp-9-2891-2009.

Wassmann, P., Reigstad, M., Haug, T., Rudels, B., Carroll, M.L., Hop, H., Gabrielsen, G.W., Falk-Petersen, S., Denisenko, S.G., Arashkevich, E., Slagstad, D., Pavlova, O., 2006. Food webs and carbon flux in the Barents Sea. Prog. Oceanogr. 71, 232–287. https://doi.org/10.1016/j.pocean.2006.10.003.

Wiedensohler, A., Birmili, W., Nowak, A., Sonntag, A., Weinhold, K., Merkel, M., Wehner, B., Tuch, T., Pfeifer, S., Fiebig, M., Fjäraa, A.M., Asmi, E., Sellegri, K., Depuy, R., Venzac, H., Villani, P., Laj, P., Aalto, P., Ogren, J.A., Swietlicki, E., Williams, P., Roldin, P., Quincey, P., Hüglin, C., Fierz-Schmidhauser, R., Gysel, M., Weingartner, E., Riccobono, F., Santos, S., Grüning, C., Faloon, K., Beddows, D., Harrison, R., Monahan, C., Jennings, S.G., O'Dowd, C.D., Marinoni, A., Horn, H.-G., Keck, L., Jiang, J., Scheckman, J., McMurry, P.H., Deng, Z., Zhao, C.S., Moerman, M., Henzing, B., de Leeuw, G., Löschau, G., Bastian, S., 2012. Mobility particle size spectrometers: harmonization of technical standards and data structure to facilitate high quality long-term observations of atmospheric particle number size distributions. Atmos. Meas. Tech. 5, 657–685. https://doi.org/10.5194/amt-5-657-2012.

Willis, M.D., Leaitch, W.R., Abbatt, J.P.D., 2018. Processes controlling the composition and abundance of Arctic aerosol. Rev. Geophys. 56, 621–671. https://doi.org/10.1029/2018RG000602.

Zangrando, R., Barbaro, E., Zennaro, P., Rossi, S., Kehrwald, N.M., Gabrieli, J., Barbante, C., Gambaro, A., 2013. Molecular markers of biomass burning in Arctic aerosols. Environ. Sci. Technol. 47, 8565–8574. https://doi.org/10.1021/es400125r.

Zhang, Q., Alfarra, M.R., Worsnop, D.R., Allan, J.D., Coe, H., Canagaratna, M.R., Jimenez, J.L., 2005. Deconvolution and quantification of hydrocarbon-like and oxygenated organic aerosols based on aerosol mass spectrometry. Environ. Sci. Technol. 39, 4938–4952. https://doi.org/10.1021/es048568l.

Zhang, Q., Jimenez, J.L., Canagaratna, M.R., Ulbrich, I.M., Ng, N.L., Worsnop, D.R., Sun, Y., 2011. Understanding atmospheric organic aerosols via factor analysis of aerosol mass spectrometry: a review. Anal. Bioanal. Chem. 401, 3045–3067. https://doi.org/10.1007/s00216-011-5355-y.